Emissive Organogel Mediated Construction of Hydrazide Linked Flexible Covalent Organic Polymer for the Separation of Aniline for Water Purification

Sayan Maiti, Tapas Ghosh, Arati Samal and Apurba K Das*

Department of Chemistry and Centre for Advanced Electronics (CAE), Indian Institute of Technology Indore, Khandwa Road, Indore 453552, India

E-mail: apurba.das@iiti.ac.in

Abstract: A flexible covalent organic polymer (**COP**) has been successfully synthesized *via* dynamic covalent gel (DCG) formation through imine condensation reaction between 6-hydrazinonicotinic hydrazide hydrate and benzene-1,3,5-tricarboxaldehyde within 7 min. Herein, an emissive organogel mediated protocol has been developed for the construction of amorphous polymer (**COP**), selectively in N,N-dimethyl acetamide (DMA). Interestingly, two non-emissive building block units have been engaged for the construction of green emissive **COP-gel**. The green emission of **COP-gel** is generated by the intermolecular H-bonding assisted aggregation induced emission phenomenon. The dried **COP** can efficiently adsorb aniline molecules into its cavities and separate them from binary mixtures of aniline/nitrobenzene and aniline/water, respectively. The UV-vis and emission spectroscopy of **COP** solution in DMA with the addition of nitrobenzene and aniline have been further investigated. The dispersion solution of **COP** in DMA shows bluish-white light emission. Photophysical investigation of **COP** in DMA suggests that the origin of the distinct emission quenching of **COP** for aniline and nitrobenzene is different. Our findings mark a significant step forward in the development of functionalized **COP** as a material for the separation of aniline from miscible binary solvent mixtures.

Introduction

Covalent organic polymers (COPs) are the unique class of organic porous material that are constructed from organic subunits into covalently linked.[1-3] Various methods or strategies have been developed to synthesize COPs. Mostly, COPs are constructed from functional organic building blocks through the formation of B-N, B-O, C=N, C=C, C-N, C=N, C=N/C-O, N=N, and Si-O bonds.[4-6] Several methods or templates such as polymer-to-polymer transformation strategy, transamination reactions of precursors, linker substitution, interfacial crystallization strategy, cyclization, utilizing a covalent organic gel formation and oxidation have been developed to synthesize COPs.[7-10] It is still a difficult task to develop alternative synthetic approaches for large-scale COPs material synthesis under ambient conditions. Aggregation assisted COPs synthetic procedure can be easiest route for the scalable COPs synthesis. In general, aggregates can be obtained after the reactions between building blocks units in three different ways through the formation of (1) crystalline covalent organic frameworks (COFs), (2) amorphous porous organic polymer and (3) gels. Gels are formed through the intermediate aggregates between crystalline COFs and amorphous COPs. However, it is a challenging task to evaluate the nature of covalent dynamic gels, despite their various applications in catalysis, sensors and adsorbent materials.[11-12]

The properties of COPs can be modified at the atomic level by using the appropriate monomers. In order to extend the implementation of porous organic polymers, time-efficient synthetic methods are being sought. Covalent organic polymers (COPs)[13-15] have received considerable importance due to their potential use in many areas, including gas storage, separation, catalysis, drug delivery and waste water purification.[16-22] In this regard, the introduction of various functional groups into porous materials have been reported as an effective way to improve their adsorption capacity and selectivity towards organic molecules. The efficient separation of aromatic organic solvent mixtures and their derivatives, which are
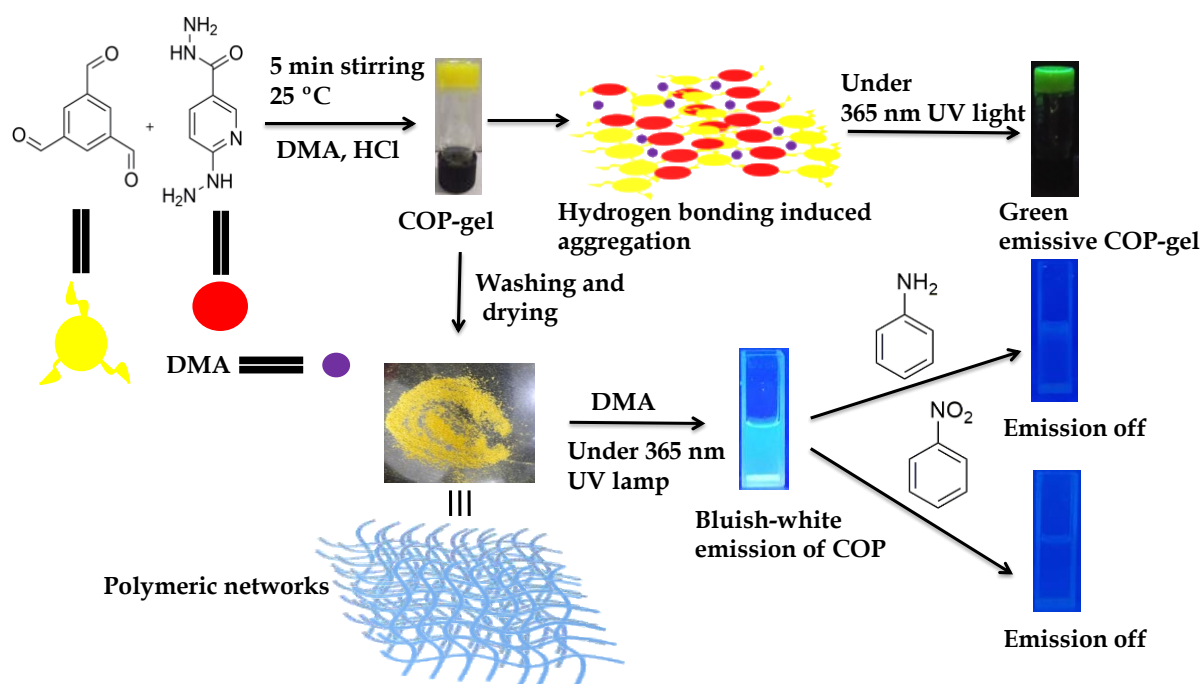
critical components of the chemical industry, can lead to higher reusability. Aniline is a crucial intermediate in the manufacture of pharmaceuticals products, rubber accelerators, and anti-aging compounds.[23] Aniline is also commonly found in the water treatment plant. Moreover, aniline is a common organic contaminant with high toxicity, rapid bio-enrichment, and challenging biodegradability.[24] Since aniline possesses potential danger in industrial scale separation, human health and environment due to their high toxicity, volatility or flammability, there is a strong demand for the development of new highly effective and environmentally safe materials for the separation of aniline from solvents mixture.[25-26] A wide range of methods and technologies have been developed to remove aniline.[27-30] On the other hand, several type of nitrogen atom containing recyclable green switchable solvents are widely used for the extraction or separation of organic solvents.[31-37] However, most of the switchable solvents are amines that separate the desire product from the solvent mixtures through a phase transition process. Li *et al* used nitrogen containing ionic liquids for the separation of binary mixture by extractive distillation methods.[38] The extractive distillation method is also allowed to separate n-heptane/ ethyl acetate and acetonitrile/ ethyl acetate mixtures.[39-41] Although above mentioned methods or processes are quite complicated and characterized by high energy consumption and high equipment cost.[41] Therefore, it is necessary to develop a convenient method and material with lower equipment costs for the separation of organic solvents. In this regard, adsorption using solid adsorbent is a quick and easy method,[27-30] and nitrogen functionalized COP can be the innovative solid adsorbent material with high adsorption capacity and selectivity for the organic solvent separation. The adsorption technique is demonstrated to be enhanced with a better adsorption capacity and selectivity due to the possible H-bonding, electrostatic and acid-base interaction between the surface functional groups on the COPs and adsorbates. Herein, our objectives are (1) to develop new synthetic methodologies with large-scale synthesis of functionalized COP

materials under ambient condition, (2) to develop cavities inside the COP backbone through dynamic covalent gel (DCG) strategy and (3) to execute the intrinsic properties of functionalized COP materials.
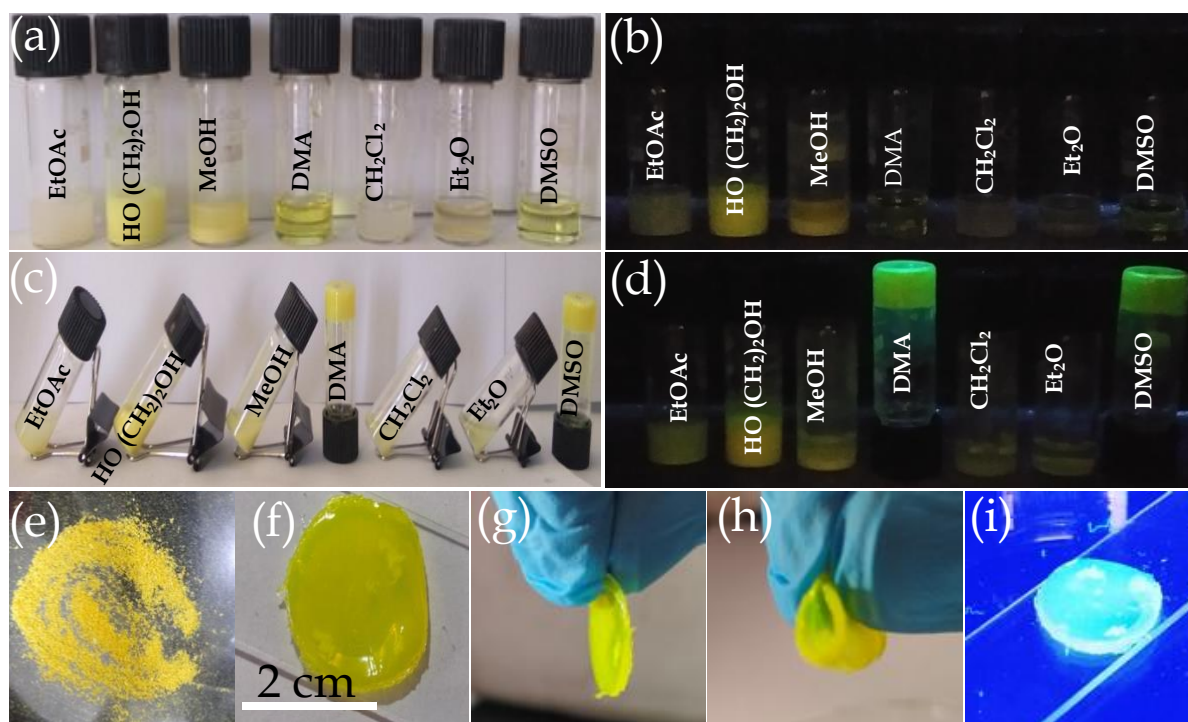
In this work, we have synthesized hydrazine, hydrazide and pyridine groups functionalized **COP** *via* emissive organogel formation within 7 min (Scheme 1). We have investigated the photophysical characteristics of emissive **COP-gel** and **COP** in DMA solution in presence of nitrobenzene and aniline. The gel formation plays a key role for synthesizing the **COP** in large scale. The **COP** is capable to adsorb or encapsulate aniline selectively in its cavities and selectively separate from binary mixtures of aniline/nitrobenzene and aniline/water (Scheme 2).

Results and Discussion

Here we have developed a facile synthetic strategy to synthesize covalent organic polymer with the 6-hydrazinonicotinic hydrazide hydrate and benzene-1,3,5-tricarboxaldehyde as building block units. Interestingly, covalent organic polymer (**COP**) was synthesized *via* organogel formation in DMA under acidic condition within 7 min (Scheme 1). The gelation formed with the **COP** concentration of about 0.038-0.040 mol L^{-1}. Among ethyl acetate (EtOAc), diethyl ether (Et_2O), ethylene glycol $(CHOH)_2$, methanol (MeOH), N,N-dimethyl acetamide (DMA), dichloromethane (CH_2Cl_2) and dimethyl sulfoxide (DMSO), **COP** has been successfully formed in DMA *via* gel formation (Figure 1). Figure S1 shows 3D block representation of **COP-gel**. To obtain pure **COP**, the **COP-gel** was dried and washed several times with water, ethyl acetate, N,N-dimethyl formamide, and methanol. After drying at 90 °C, the **COP** was characterized using several techniques.

Scheme 1 (a) Schematic representation of porous **COP** synthesis, and aniline separation and adsorption by **COP**.
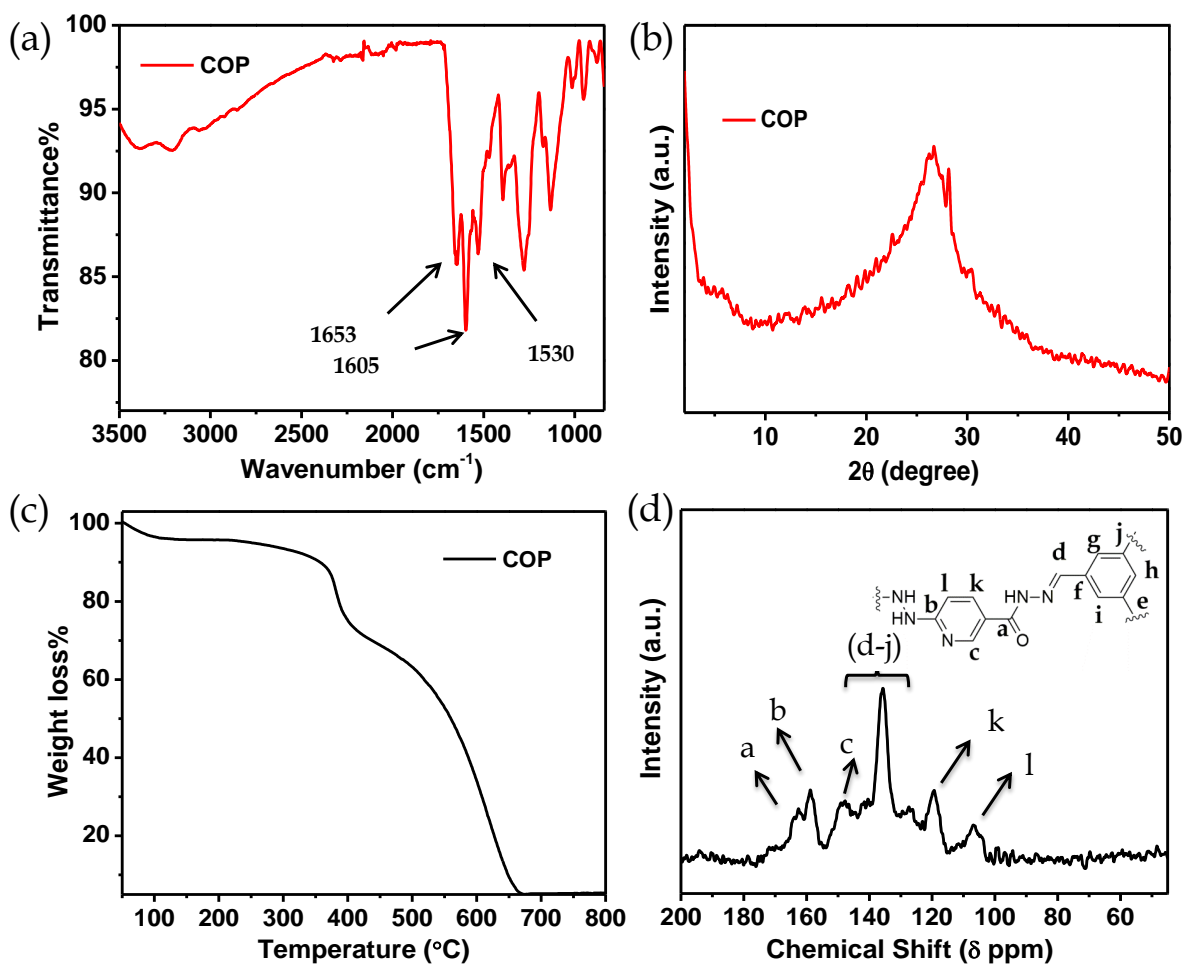

Figure 1. Solution mixture of 6-hydrazinonicotinic hydrazide hydrate and benzene-1,3,5-tricarboxaldehyde in different solvents (a) in day light and (b) under 365 nm UV light. Solution mixture of 6-hydrazinonicotinic hydrazide hydrate and benzene-1,3,5-tricarboxaldehyde in different solvents after the addition of 1N HCl (c) in day light and (d)

under 365 nm UV light. Optical images of (e) **COP** powder, (f-h) Thin film form of **COP** and (i) **COP** thin film (shows white- cyan color emission) under 365 nm UV light.
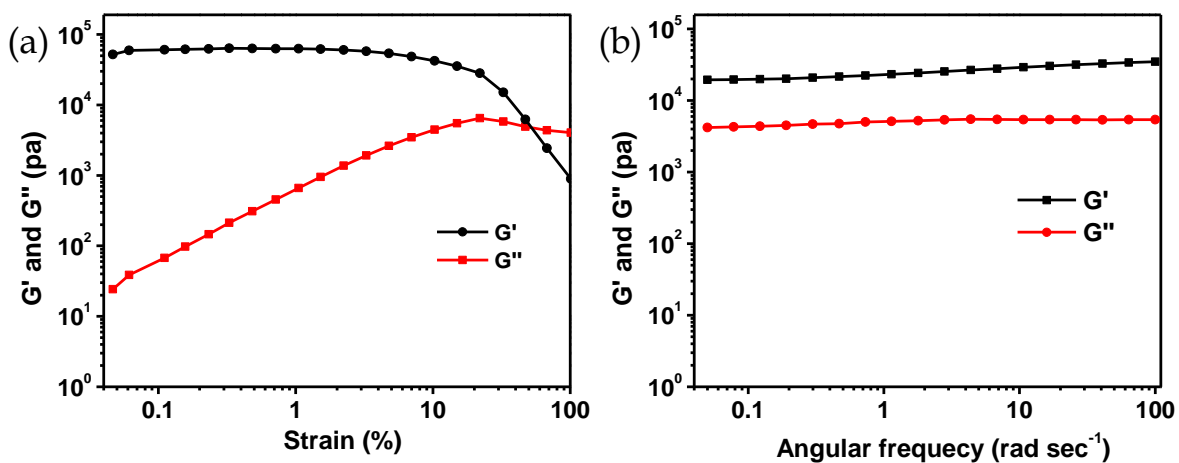
The FT-IR spectrum of **COP** demonstrates the successful construction of **COP** *via* the -C=N bond formation between their building block units. Similar kinds of FT-IR spectra indicate that **COP** has identical functionalities and linkages.[42-44] The peaks at 1530, 1605 cm^{-1} are assigned to -C=C- and -C=N bonds stretching. A peak at 1650 cm^{-1} is appeared due to -C(=O)NHNH- stretching band (Figure 2a). The powder XRD pattern of **COP** suggests that the polymer is successfully constructed from two crystalline secondary building block units (Figure S2a). The broad powder XRD pattern of **COP** assigns its amorphous polymeric nature (Figure 2b). A slight broad peak at higher 2θ indicates to the strong π-π stacking interaction between the **COP** layers. To account the thermal stability of **COP**, we have performed thermogravimetric analysis (Figure 2c). The **COP** exhibits high thermal stability. The TGA spectrum of COP shows a 4% weight loss at lower temperature range from 27 to 200 °C due to the evaporation of residual solvents, followed by the weight loss of 6.34% and 15.95% over the temperature range of 200 to 370 °C and 370 to 402 °C respectively. Following that, a gradual loss of weight is observed as the temperature goes up.

The solid-state ^{13}C CP-MAS NMR of **COP** also supports the successful formation of COP (Figure 2d). The peaks from 120-140 ppm confirm the presence of the phenyl groups. The peak at 159 ppm suggests acylhydrazone groups in **COP**. The peak at 163 ppm confirms the presence carbonyl group of -C(O)NHNH- and a peak at 150 ppm is appeared due to C=N bond of pyridine ring.[44] The porosity of COP was evaluated by performing BET surface area analysis by N$_2$ sorption at 77 K and 1 bar pressure. No hysteresis loop is observed in the isotherm. The **COP** shows type II reversible isotherm (Figure S2b). The presence of micropores is demonstrated by a steep uptake at a low relative pressure P/P$_0$. This result clearly suggests that microporosity has been grown inside the **COP** during the gel formation.

At high relative pressures of $P/P_0 > 0.9$, a significant volume of N_2 adsorption is observed. The increase in N_2 adsorption at $P/P_0 > 0.9$ and the complete absence of saturation in the adsorption isotherm can be ascribed to the condensation of nitrogen gas molecules in inter-particular voids or in larger pores. The calculated surface area of **COP** is 645.9 $m^2 g^{-1}$ (Table S1). The pore size distribution of **COP** was studied *via* NLDFT method (Figure S3). The calculated pore volume of **COP** is 0.49 cc.g^{-1}. The rheology of **COP-gel** has been performed to evaluate the mechanical properties of **COP-gel** (Figure 3). This experiment is carried out at ambient temperature. The oscillatory frequency has been performed at frequency range of 0.05 to 100 rad s^{-1} for an applied strain of 1%. The storage modulus (G') is significantly higher than the loss modulus (G'') over the studied frequency range which clearly indicates the viscoelastic and robustness nature of **COP-gel**. According to scanning (SEM) and high resolution transmission electron microscopy (HRTEM), **COP** generates a sponge-like porous structure made up of interconnected nanoscale spherical particles (Figure 4a and 4b). The particles with a diameter of 20-40 nm combine to form a three-dimensional gel matrix.

The surface hydrophobicity and surface roughness of **COP** was evaluated using atomic force microscopy (Figure 4c). The nano level surface roughness illustrates the hydrophobicity of **COP**. Generally, highly hydrophobic materials have tendency to aggregate into spherical assembly upon coating on glass surface.[45] Similarly, the COP also shows this salient features.
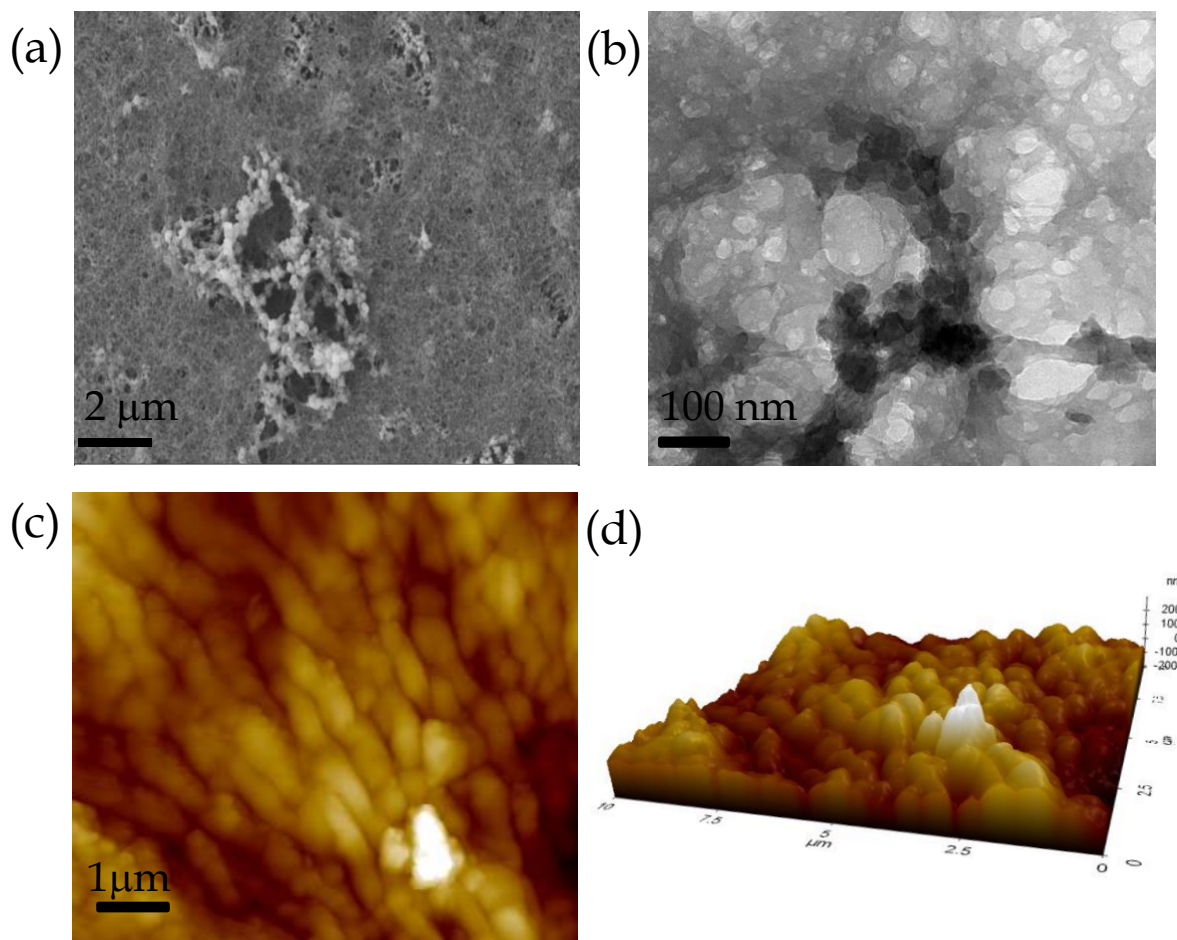
Figure 2. (a) FT-IR spectrum of **COP**. (b) Powder XRD pattern of **COP**. (c) TGA of **COP**. (d) Solid state ^{13}C NMR spectrum NMR of **COP**.

Figure 3. (a) Linear viscoelastic (LVE) properties of (a) **COP**-gel and (b) the dynamic frequency sweep experiment of **COP**-gel.

Figure 4. (a) SEM, (b) HRTEM images of **COP**. (c) AFM image of **COP** and (d) 3D AFM (Z-axis interpretation) image of **COP**.

The **COP** surface contains several crests and troughs (Figure 4d) which have been observed from 3D view (Figure 4d). The peaks in the region of 0.5 μm indicate the existence of air pockets between the peaks (valley regions). These trapped air pocket in the valley region creates the hydrophobic pore in **COP**.

Photophysical Investigation of COP-gel

The **COP**-gel shows green emission within the range of 520-550 nm. Interestingly two secondary building block units are non-fluorescent in DMA solvent and the pyridine moiety is itself a fluorescence quencher. The **COP** backbone is rigidified through a series of H-bonding interaction between the hydrazide groups and the solvent molecule (DMA) (Figure

S4). These H-bonds are highly responsible for the restriction of intramolecular rotation, which causes aggregation-induced emission (AIE).[46-47] The emission color of **COP** originates from distinct level of aggregation in solvent mixture which alters the electronic distribution and shows different fluorescent color. So, H-bonding plays a significant role in the evolution of emissive **COP-gel**. By varying the concentration of building block units, we have also prepared **COP** through flexible thin film preparation in DMA solvent. Different extent of aggregation is occurred in gel and thin film that leads different emission colors (Figure 1g and 1i). We have investigated detailed spectroscopic study to prove the H-bonding induced strong aggregation in **COP-gel**. The UV-vis spectrum of **COP-gel** shows an absorption maximum centered at 311 nm, which is attributed to the n-σ* transition (Figure S5). On the other hand, an absorption peak at 423 nm of **COP-gel** is observed, which suggests the formation of strong intermolecular hydrogen bonds. This phenomenon indicates its higher order aggregated state by restricting intramolecular rotation (RIR) and lowering the HOMO-LUMO energy gap.[48-49] Also, a broader absorption band reveals higher order aggregated form of **COP**-gel (Figure S5). The **COP**-gel shows dual emission at 517 nm with a shoulder peak at 621 nm (Figure S6). We have also performed temperature dependent fluorescence studies of **COP**-gel. The temperature-dependent fluorescence studies reveal that emission intensity decreases gradually with the increase in temperature (Figure S7). These results also support the existence of H-bonding inside the **COP-gel**.

The excitation spectrum of **COP-gel** at 517 nm is similar with the excitation spectrum of **COP-gel** at 621 nm (Figure S8). These results indicate that the origin of shoulder band at around 621 nm of **COP**-gel is assigned to the protonated state.[50] An emission peak at 621 nm originates from the protonated form of the **COP-gel** (due to formation of the PyH^+ and imine -C=NH^+-). The green color emission of **COP-gel** is also visualized under confocal microscope with the excitation wavelength of 405 nm and emission collection of 540 nm
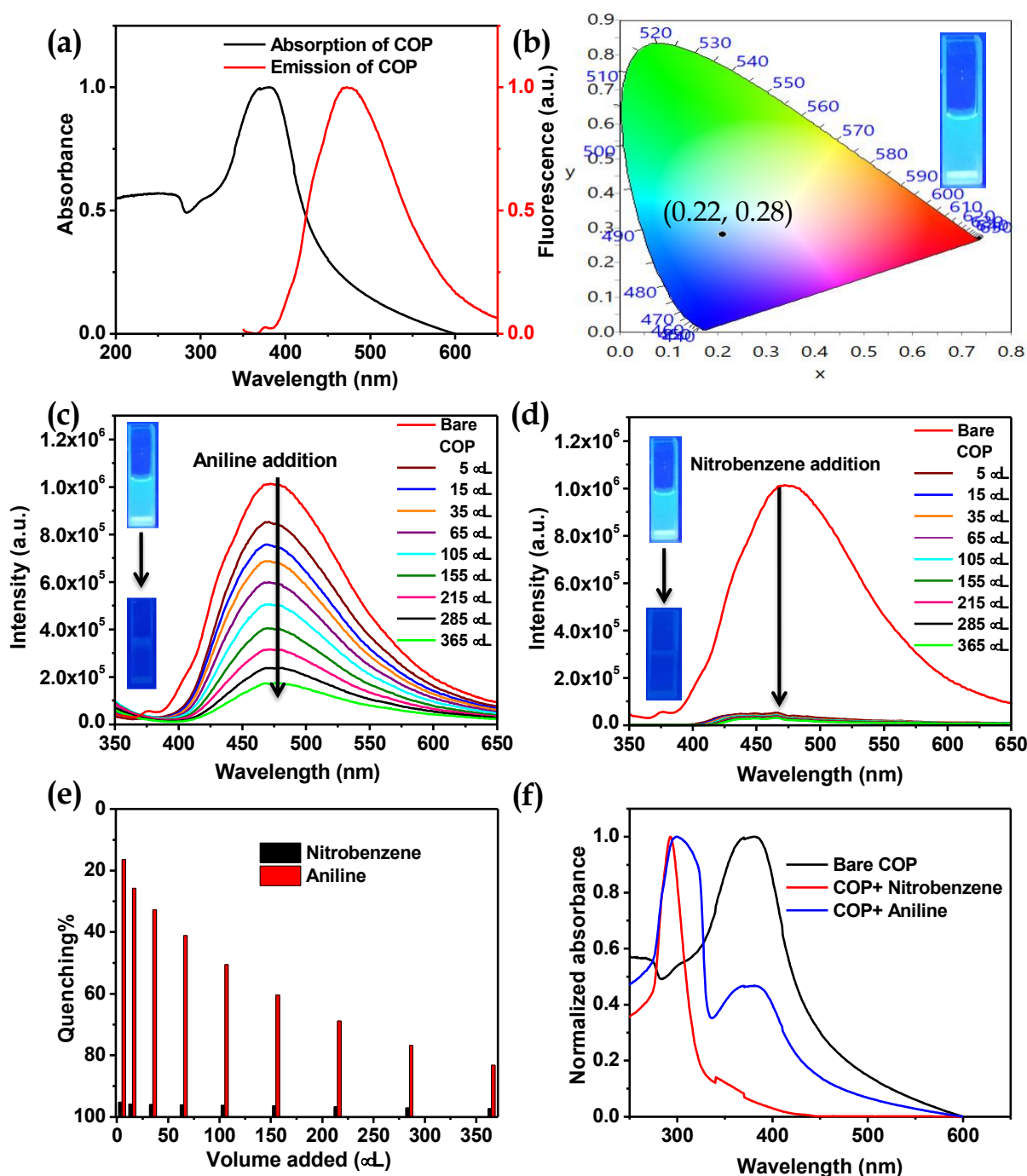
respectively. The confocal image of **COP** is shown in Figure S9. Confocal images further support the AIE phenomenon in solid state of **COP** in green color region.[51] To find out further information into the photophysical behaviour of **COP**-gel, fluorescence decay measurements were performed. Figure S10 represents the fluorescence decay curves of **COP**-gel. The decays do not fit well with single or bi-exponential function rather fit well with a tri-exponential function. The average lifetime is 0.43 ns and 0.5 ns for the emissions from **COP**-gel at 517 and 621 nm (Table S1). The average lifetime of the protonated **COP-gel** emission is little longer than the normal emission.

Photophysical Investigation of COP Solution in DMA Solvent

We have further investigated the photophysical properties of disperse solutions of **COP** powder in DMA solvent. As previously stated, the introduction of hydrazide functionality is crucial for strengthening the **COP**'s emissive behaviour *via* strong intra- and interlayer H-bonding interactions. In the UV-vis spectra of **COP** solution, a broad absorption maximum is found across the wavelength range of 300 to 400 nm, which correlates to the n-π^* transitions and also reveals its aggregated state (Figure 5a). For an excitation wavelength of 340 nm, the emission spectra of **COP** in DMA shows a maximum at 474 nm (Figure 5a), which may be placed at (0.22, 0.28) in CIE coordinates, indicating that it is close to a blue-white light emission zone (Figure 5b). Pyridine and hydrazide functionalized **COP** showcased adequate thermal and chemical stability due to the presence of several heteroatoms in the polymeric backbone, and H-bonding controlled fluorescence property in DMA solution. The abundant heteroatoms form intra- and intermolecular H-bonds, causing aggregation, limiting intermolecular rotation, and emitting light. The emission intensity of **COP** is highest in DMA solution, which is clearly attributed to intermolecular or intermolecular H-bonding assisted aggregation induced emission properties. The **COP**'s significant emissive behavior and

numerous chelating or interacting sides influence us to explore its sensing application as a fluorescent chemosensor for several aromatic molecules in DMA. Herein, we have investigated the effect of nitro and amine groups containing aromatic compounds on the aggregation induced emission properties of **COP** in DMA solution. Nitrobenzene and aniline have been used for the experiment. Nitrobenzene, and aniline were added in a specific series of volumes into the disperse solution of **COP** in DMA. To investigate the sensing ability of **COP** toward different aromatic derivatives in DMA solution, the fluorescence titration measurements were carried out with the gradual addition of nitrobenzene and aniline (5 to 365 μL). The result indicates that aniline and nitrobenzene cause an obvious quenching effect on the emission intensity of **COP** dispersed in DMA solution (Figure 5c and 5d). The **COP** shows higher degree of quenching effect for nitrobenzene than aniline (Figure 5e). Thus, **COP** could be applied as an efficient fluorescence sensor for the detection of nitrobenzene. The emission intensity of **COP** dispersed in **DMA** is quenched drastically upon incremental addition of 5 μL of nitrobenzene by 95%, respectively, while low quenching is observed for aniline. The fluorescence of **COP** is almost quenched (98%) after addition of 365 μL of nitrobenzene. After adding 5 μL of aniline, only 16% of the fluorescence quenching of **COP** is observed. Nitrobenzene has a higher order of quenching efficiency, distinguishing it from -NH$_2$ containing aniline. The ground state aggregated absorption peak of **COP** near 400 nm is drastically diminished in the presence of nitrobenzene, which is attributed to the collapse of these aggregated states due to the interaction with nitrobenzene (Figure 5f). As a result, in the presence of nitrobenzene, we found a quick drop in the fluorescence window of **COP**, indicating that the aggregated form of **COP** is the source of emission properties. On the other hand a gradual decrease of emission intensity and static quenching of **COP** is observed in addition of aniline. This result is attributed to the formation of ground state association of aniline with the aggregated state of the **COP** in DMA.[52] The excitation spectra of **COP**

solution in presence of aniline and nitrobenzene also support our statement (Figure S11). The excitation spectrum of **COP** at 474 nm is similar with the excitation spectrum of **COP** at 474 nm in presence of aniline. On the other hand, the excitation spectrum of **COP** at 474 nm differs significantly from the excitation spectrum of **COP** at 474 nm in the presence of nitrobenzene. These findings suggest that the source of distinct emission quenching of **COP** solution in DMA for aniline and nitrobenzene is different.
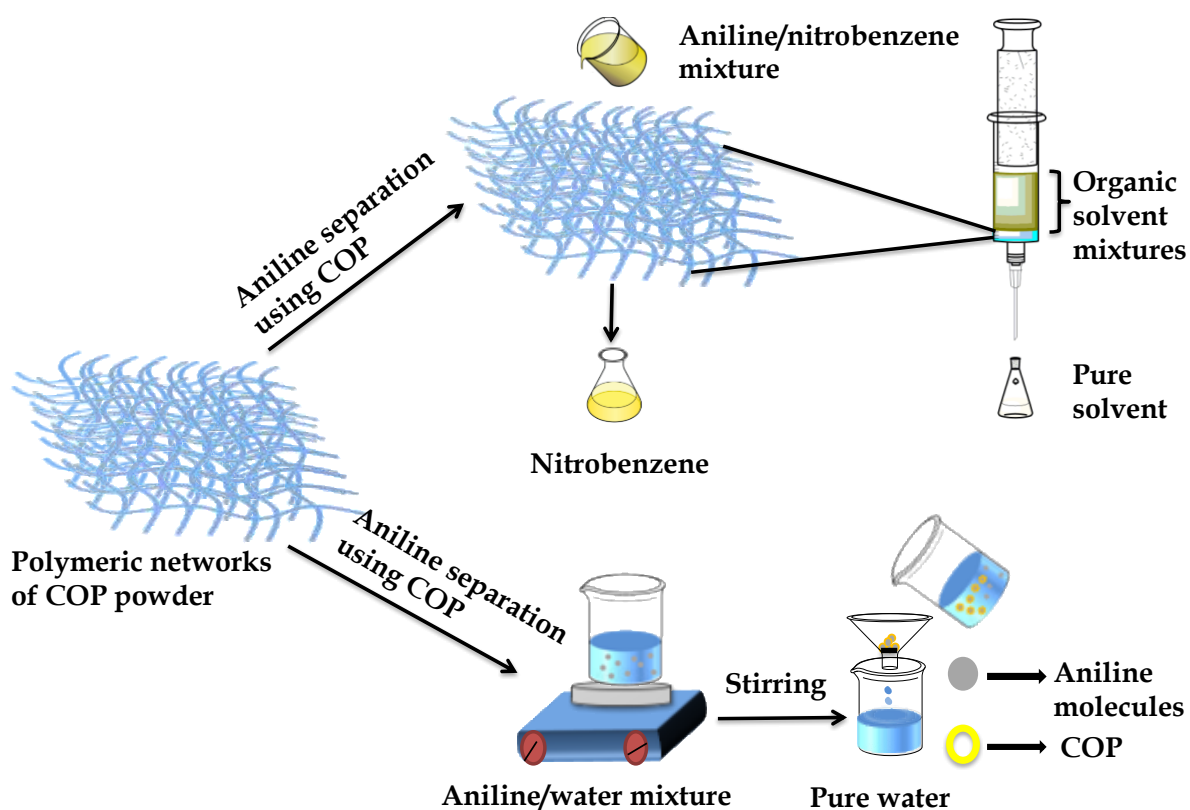
Figure 5. (a) Absorption and emission spectra of **COP** in DMA. (b) Corresponding CIE diagram of **COP** solution in DMA. (c) Emission quenching of **COP** in addition of aniline (λ_{ex} = 340 nm). (d) Emission quenching of **COP** in addition of nitrobenzene (λ_{ex} = 340 nm). (e) Degree of emission quenching of **COP** in presence of aniline and nitrobenzene. (f) UV-vis of **COP** in addition of nitrobenzene (2 μL) and aniline (10 μL).

Separation and Extraction of Aniline from the Binary Solvent Mixture

Solvent extraction method is widely used to isolate aromatic organic solvent mixtures and their derivatives. The choice of material is highly influenced by its similarity to the target product, cost and safety. Nitrogen-rich switchable materials, a type of recyclable green materials, can be used to separate the organic solvent mixtures in efficient cost-effective manner.[53] Herein, the **COP** acts as an efficient stationary phase for the separation of organic solvents from binary organic solvent mixtures (Scheme 2 and Figure S12). We have taken aniline/nitrobenzene as model organic solvent mixture for the separation experiment using dried **COP**. Initially, we loaded 60 mg of **COP** inside 1 mL (5.5 cm) glass syringe and packing length was 0.15 mL (0.7 cm). At first, we took 50 μL of each solvent and diluted it with hexane and passed through the **COP** loaded in 1 mL glass syringe. The **COP** selectively adsorb and separate aniline from nitrobenzene. Hexane was used as mobile phase solvent. All the filtrates were characterized by high performance liquid chromatography (HPLC) (Figure S13-S14). Generally, separation of the organic solvents depend on the surface charge of the **COP**, pore size, functionality on the **COP** surface and electrostatic interactions between **COP** and organic solvents. Here, the **COP** exhibits hydrazide and pyridinic groups rich surface with average pore size distribution of 1.3 to 10 nm.[54-55] Aniline shows high binding interactions and easily stack with the **COP** backbone through -NH⋯N- interactions that also induces the aggregation properties of **COP** and reside in the pore cavity of the polymer.[56-63] Nitrobenzene, on the other hand, lacks any polar amine (-NH$_2$) group and is unable to bind

with the **COP** backbone; rather, it collapses the **COP** assembly that is supported by the UV-vis spectra of **COP** in DMA solution (Figure 5f). As a result, nitrobenzene can easily escape *via* the **COP**. Hexane (6 mL) is required to remove the entire amount of nitrobenzene. We have also investigated the adsorption limit of aniline over 60 mg **COP** powder. The adsorption limit of **COP** is found as 55 µL/60 mg for aniline. After each cycles, loaded **COP** powder (stationary phase) was washed very well with the water, ethyl acetate and methanol to remove adsorbed solvent (aniline) from the pore of **COP**. After that used **COP** was dried under 90 ºC temperature and used for next cycle. The **COP** was reused and the **COP** retains its activity after five cycles (Figure S15).

Scheme 2. Aniline separation from binary solvent mixtures aniline/nitrobenzene and aniline/water.

For the purpose of the extraction of aniline from aniline/water mixture, we have directly used the resultant **COP** powder. The adsorption mechanism was followed to extract aniline where

COP acts as adsorbent for the aniline in aqueous solution. Here, 45 mg of **COP** powder was added to a 3 mL aqueous solution of aniline with the concentration of 222 mg L^{-1} and allowed to stir at 25 °C. UV-Vis spectra of the resultant solution were recorded at different time intervals. The gradual decrease in aniline absorbance suggests quick adsorption performance (Fig. S16a). The **COP** exhibits significant adsorption performance for aniline, removing 83.5% of aniline in 8 h and achieves adsorption equilibrium (using Eq. S1).

The removal rate of **COP** for aniline is substantially higher, implying that -NH$_2$ group of aniline plays a crucial role in the adsorption process towards **COP** functionalities. Compared with the nitrobenzene, the **COP** is the better adsorbent material with fast adsorption for aniline, which is due to the well-defined porous structure and surface functionalities. The adsorption process demonstrates that the incorporated hydrazide groups of **COP** are favourable for adsorption due to possible hydrogen bonding and acid-base interactions. To further investigate the adsorption kinetics, the adsorption of aniline was recorded (q_t) at different time intervals (Fig. S16b and c), where q_t represents the corresponding adsorption at specific time t (Eq. S2). The **COP** achieves a maximum aniline adsorption capacity (q_e) of 12.5 mg g^{-1} (using Eq. S2). The pseudo-second-order rate constant was investigated to simulate the adsorption kinetics of **COP** for aniline, and the linear forms of the pseudo-second order kinetics model for aniline is expressed by Eq. S3 (Fig. S16d). The initial adsorption rate, ($k_2 q_e^2$), is calculated as 2.5 mg g^{-1} h^{-1}. It is demonstrated that the kinetic data agree well with the pseudo second-order model. Even after third adsorption cycles, **COP** still can remove more than 60% of aniline from the aqueous solution.

Conclusion

In summary, we synthesized covalent organic polymer (**COP**) *via* dynamic covalent gel (DCG) through imine bond formation between 6-hydrazinonicotinic hydrazide hydrate and

benzene-1,3,5-tricarboxaldehyde within 7 min. DMA solvent showed a significant role for the scalable synthesis of **COP** *via* gel formation. The emissive gel served as an interesting protocol for the porous **COP's** construction. The **COP-gel** exhibited green emission. The green emission of **COP-gel** was caused by an aggregation-induced emission phenomenon, which was assisted by H-bonding and several non-covalent interactions. On the other hand, the disperse solution of **COP** in DMA showed bluish-white light emission. The degree of aggregation was important in determining the emission colour of **COP** in gel and solution states. The dried **COP** had the ability to easily adsorb aniline molecules into its cavities and separate them from binary mixtures of aniline/nitrobenzene and aniline/water. The UV-vis and emission spectroscopy of **COP** solution in DMA with the addition of nitrobenzene and aniline had been further investigated. Our findings represent a significant advancement in the development of functionalized COP with excellent scalability under ambient conditions, as well as significant physical insights for the separation of aniline from miscible binary solvent mixtures.

References

[1] P. Puthiaraj, Y.-R. Lee, S. Zhang, W.-S. Ahn, *J. Mater. Chem. A*, **2016**, *4*, 16288-16311.
[2] Z. Xiang, D. Cao, L. Dai, *Polym. Chem.*, **2015**, *6*, 1896-1911.
[3] K. Geng, T. He, R. Liu, S. Dalapati, K. T. Tan, Z. Li, S. Tao, Y. Gong, Q. Jiang, D. Jiang, *Chem. Rev.* **2020**, *120*, 8814-8933.
[4] V. S. Vyas, F. Haase, L. Stegbauer, G. Savasci, F. Podjaski, C. Ochsenfeld,B. V. Lotsch, *Nat. Commun.* **2015**, *6*, 8508.
[5] P. Wang, F. Zhou, C. Zhang, S.-Y. Yin, L. Teng, L. Chen, X.-X. Hu, H. W.Liu, X. Yin, X.-B. Zhang, *Chem. Sci.* **2018**, *9*, 8402–8408.

[6] F. Haase, K. Gottschling, L. Stegbauer, L. S. Germann, R. Gutzler, V.Duppel, V. S. Vyas, K. Kern, R. E. Dinnebier, B. V. Lotsch, *Mater. Chem. Front.* **2017**, *1*, 1354–1361.

[7] Z. Miao, G. Liu, Y. Cui, Z. Liu, J. Li, F. Han, Y. Liu, X, Sun, X. Gong, Y. Zhai, Y. Zhao, Y. Zeng, *Angew. Chem., Int. Ed.* **2019,** *58*, 4906-4910.

[8] C. Qian, Q.-Y. Qi, G.-F. Jiang, F.-Z. Cui, Y. Tian, X. Zhao, *J. Am. Chem. Soc.* **2017**, *139*, 6736-6743.

[9] W. Luo, Y. Zhu, J. Zhang, J. He, Z. Chi, P. W. Miller, L. Chena, C.-Y. Su, *Chem. Commun.* **2014**, *50*, 11942- 11945.

[10] K. Dey, M. Pal, K. C. Rout, S. Kunjattu, A. Das, R. Mukherjee, U. K. Kharul, R. Banerjee, *J. Am. Chem. Soc.* **2017**, *139*, 13083-13091.

[11] H. Fang, L. Chen, L. Zeng, Z. Yang, J. Zhang, *Global Challenges* **2019**, *3*, 1800073.

[12] H. Zhong, Y. Gong, W. Liu, B. Zhang, S. Hu, R. Wang, *Dalton Trans.* **2019**, *48*, 2345-2351.

[13] S. Das, P. Heasman, T. Ben, S. Qiu, *Chem. Rev.* **2017**, *117*, 1515–1563.

[14] L. Tan, B. Tan, *Chem. Soc. Rev.* **2017**, *46*, 3322–3356.

[15] H. Bildirir, V. G. Gregoriou, A. Avgeropoulos, U. Scherf, C. L. Chochos, *Mater. Horiz.* **2017**, *4*, 546–556.

[16] W. Wang, M. Zhou, D. Yuan, *J. Mater. Chem.* A **2017**, *5*, 1334-1347.

[17] Q. Chen, M. Luo, P. Hammershøj, D. Zhou, Y. Han, B. W. Laursen, C. Yan, B. Han, *J. Am. Chem. Soc.* **2012**, *134*, 6084–6087.

[18] Y. Yuan, F. Sun, L. Li, P. Cui, G. Zhu, *Nat. Commun.* **2014**, *5*, 4260.

[19] Q. Sun, Z. Dai, X. Meng, L. Wang, F. Xiao, *ACS Catal.* **2015**, *5*, 4556-4567.

[20] M. H. Alkordi, L. J. Weselinski, V. D'Elia, S. Barman, A. Cadiau, M. N. Hedhili, A. J. Cairns, G. AbdulHalim, J. Basset, M. Eddaoudi, *J. Mater. Chem. A* **2016**, *4*, 7453-7460.

[21] Y. Zhang, S. N. Riduan, *Chem. Soc. Rev.* **2012**, *41*, 2083-2094.

[22] Q.Fang, J.Wang,S.Gu, R. B.Kaspar, Z.Zhuang, J. Zheng, H. Guo, S. Qiu, Y. Yan, *J. Am. Chem. Soc.* **2015**, *137*, 8352-8355.

[23] D.-W. Gao, Q. Hu, H. Pan, J. Jiang, P. Wang, *Biores. Technol.* **2015**, *193*, 507-512.

[24] F. An, X. Feng, B. Gao, *J. Hazard. Mater.* **2010**, *178*, 499-504.

[25] K. Yang, W. Wu, Q. Jing, L. Zhu, Environ. *Sci. Technol.* **2008**, *42*, 7931-7936.

[26] Y. Zhou, X. Gu, R. Zhang, J. Lu, *Ind. Eng. Chem. Res.* **2014**, *53*, 887-894.

[27] Y. Chen, B. Wang, X. Wang, L.-H. Xie, J. Li, Y. Xie, J.-R. Li, *ACS Appl. Mater. Interface* **2017**, *9*, 27027-27035.

[28] S. H. Gheewala, A. P. Annachhatre, *Water Sci. Technol.* **1997**, *36*, 53-58 .

[29] L. Wang, J. Guo, X. Xiang, Y. Sang, J. Huang, *Chem. Eng. J.* **2020**, *387*, 124070.

[30] S. Luo, Q. Zhang, Y. Zhang, K. P. Weaver, W. A. Phillip, R. Guo, *ACS Appl. Mater. Interface* **2018**, *10*, 15174-15182.

[31] P. G. Jessop, S. M. Mercer, D. J. Heldebrant, *Energy Environ. Sci.* **2012**, *5*, 7240-7253.

[32] G. J. Philip, L. Phan, A. Carrier, S. Robinson, J. D. Christoph, R. H. Jitendra, *Green Chem.* **2010**, *12*, 809-814.

[33] P. G. Jessop, C. A. Eckert, C. L. Liotta, D. J. Heldebrant, *US Pat.* 2008/005849A1, United States Patent Application Publication, 2008.

[34] J. Durelle, J. R. Vanderveen, Yi Quan, C. B. Chalifoux, J. Kostin, P. G. Jessop, *Phys. Chem. Chem. Phys.* **2015**, *17*, 5308-5313.

[35] C. Samor`ı, L. Pezzolesi, D. L´opez Barreiro, A. Quintavalla, A. Pasteris, E. Tagliavini, *RSC Adv.* **2014**, *4*, 5999-6008.

[36] P. Pollet, C. A. Eckert, C. L. Liotta, *Chem. Sci.* **2011**, *2*, 609-614.

[37] A. D. Wilson, F. F. Stewart, *RSC Adv.* **2014**, *4*, 11039-11049.

[38] W. Li, B. Xu, Z. Lei, C. Dai, *Chem. Eng. Process.* **2018**, *126*, 81-89.

[39] W. Ma, J. Sun, W. Hongpu, R. Wang, *Appl. Chem. Ind.* **2010**, *39*, 781-782.

[40] W. Kang, M. Li, Y. Wu, J. Cheng, R. Gao, *Mod. Chem. Ind*. **2017**, *37*, 167-170.

[41] J. Gu, X. You, C. Tao, J. Li, W. Shen, J. Li, *Chem. Eng. Res. Des*. **2018**, *133*, 303-313.

[42] F. J. U.-Romo, C. J. Doonan, H. Furukawa, K. Oisaki, O. M. Yaghi, *J. Am. Chem. Soc*. **2011**, *133*, 11478-11481;

[43] S. Maiti, A. Roy Chowdhury, A. K. Das, *ChemNanoMat.* **2019**, *6*, 99-106.

[44] S. Maiti, B. Mandal, M. Sharma, S. Mukherjee, A. K. Das, *Chem. Commun*. **2020**, *56*, 9348-9351.

[45] A. Roy Chowdhury, S. Maiti, A. Mondal, A. K. Das, *J. Phys. Chem. C* **2020**, *124*, 7835-7843.

[46] S. Dalapati, E. Jin, M. Addicoat, T. Heine, D. Jiang, *J. Am. Chem. Soc*. **2016**, *138*, 18, 5797-5800.

[47] D. Wang, S.-M. Li, Y.-F. Li, X.-J. Zheng, L.-P. Jin, *Dalton Trans*. **2016**, *45,* 8316-8319.

[48] S. Riebe, C. Vallet, F. v. Vight, D. G.-Abradelo, C. Wölper, P.-D. C. A. Strassert, G. Jansen, S. Knauer, J. Voskuhl, *Chem. Eur. J*. **2017**, *23*, 13660-13668.

[49] H.-Q. Yin, F. Yin, X.-B. Yin, *Chem. Sci*. **2019**, *10*, 11103-11109.

[50] F.-Z. Cui, J.-J. Xie, S.-Y. Jiang, S.-X. Gan, D.-L. Ma, R.-R. Liang, G.-F. Jiang, X. Zhao, *Chem. Commun*. **2019**, *55*, 4550-4553.

[51] S. Feng, S. Gong, G. Feng, *Chem. Commun*. **2020**, *56*, 2511-2513.

[52] L. Deng, X. Kang, T. Quan, L. Yang, S. Liu, K. Zhang, M. Gao, Z. Xia, D. Gao, *ACS Appl. Mater. Interfaces* **2021**, *13*, 33449-33463.

[53] Y. Liu, Z. Qiu, H. Zhong, X. Zhao, W. Huang, X. Xing, *RSC Adv*. **2020**, *10*, 12953-12961.

[54] S. Ravi, P. Puthiaraj, K. Yu, W.-S. Ahn, *ACS Appl. Mater. Interfaces* **2019**, *11*, 11488-11497.

[55] P. Song, Z. Zhang, L. Yu, P. Wang, Q. Wang, Y. Chen, *New J. Chem*. **2020**, *44*, 8572-8577.

[56] J.-X. Zhou, X.-S. Luo, X. Liu, Y. Qiao, P. Wang, D. Mecerreyes, N. Bogliotti, S.-L. Chen, M.-H. Huang, *J. Mater. Chem. A* **2018**, *6*, 5608-5612.

[57] Y. Liu, X. Fan, X. Jia, B. Zhang, H. Zhang, A. Zhang, Q. Zhang, *J. Mater. Sci*. **2016**, *51*, 8579-8592.

[58] A. R. A. Hamid, R. Mhanna, R. Lefort, A. Ghoufi, C. Alba-Simionesco, B. Frick, D. Morineau, *J. Phys. Chem. C* **2016**, *120*, 9245-9252

[59] C. A. Hunter, *J. Mol. Biol*. **1993**, *230*, 1025-1054.

[60] S. K. Burley, G. A. Petsko, *Science* **1985**, *229*, 23-28.

[61] M. Falkowska, D. T. Bowron, H. Manyar, T. G. A. Youngs, C. Hardacre, *Angewandte Chemie International Edition* **2018**, *57*, 4565-4570.

[62] J. Huang, X. Han, S. Yang, Y. Cao, C. Yuan, Y. Liu, J. Wang, Y. Cui, *J. Am. Chem. Soc*. **2019**, *141*, 8996-9003.

[63] P. Das, G. Chakraborty, S. K. Mandal, *ACS Appl. Mater. Interfaces* **2020**, *12*, 10224-10232.